Crystal Structures of the Scaffolding Protein LGN Reveal the General Mechanism by Which GoLoco Binding Motifs Inhibit the Release of GDP from Gα$_i$*

Min Jia[‡§1], **Jianchao Li**[¶1], **Jinwei Zhu**[‡¶], **Wenyu Wen**[‡], **Mingjie Zhang**[¶‖2], and **Wenning Wang**[‡3]

From the ‡Shanghai Key Laboratory of Molecular Catalysis and Innovative Materials, Department of Chemistry and Institute of Biomedical Sciences and the §Department of Pharmacy, Fudan University, Shanghai 200433, China and the ¶Division of Life Science, State Key Laboratory of Molecular Neuroscience and the ‖Center of Systems Biology and Human Health, Hong Kong University of Science and Technology, Clear Water Bay, Kowloon, Hong Kong, China

Background: GoLoco (GL) motif binds to Gα and inhibits its guanine nucleotide dissociation.

Results: Crystal structures of LGN-GL3(4)·Gα$_{i1(3)}$ complexes reveal a double Arg finger-mediated GDP recognition mechanism, which is distinct from that shown in the RGS14·Gα$_{i1}$ complex.

Conclusion: LGN-GL/Gα$_i$ interaction might represent a general binding mode between GoLoco motifs and Gα$_i$.

Significance: Our findings shed new light on the GoLoco motif-mediated G protein signaling regulation.

GoLoco (GL) motif-containing proteins regulate G protein signaling by binding to Gα subunit and acting as guanine nucleotide dissociation inhibitors. GLs of LGN are also known to bind the GDP form of Gα$_{i/o}$ during asymmetric cell division. Here, we show that the C-terminal GL domain of LGN binds four molecules of Gα$_i$·GDP. The crystal structures of Gα$_i$·GDP in complex with LGN GL3 and GL4, respectively, reveal distinct GL/Gα$_i$ interaction features when compared with the only high resolution structure known with GL/Gα$_i$ interaction between RGS14 and Gα$_{i1}$. Only a few residues C-terminal to the conserved GL sequence are required for LGN GLs to bind to Gα$_i$·GDP. A highly conserved "double Arg finger" sequence (RΨ(D/E)(D/E)QR) is responsible for LGN GL to bind to GDP bound to Gα$_i$. Together with the sequence alignment, we suggest that the LGN GL/Gα$_i$ interaction represents a general binding mode between GL motifs and Gα$_i$. We also show that LGN GLs are potent guanine nucleotide dissociation inhibitors.

The α subunit of the heterotrimeric G proteins (Gα) is a critical component of the G protein signaling pathway, in which Gα cycles between the GDP- and GTP-bound states (1). In the canonical signaling model, ligand-mediated activation of G protein-coupled receptors (GPCRs)[4] catalyzes the exchange of GDP for GTP in binding to Gα and subsequently results in the dissociation of Gα·GTP from Gβγ heterodimer (2, 3). The dissociated Gα·GTP binds to and activates downstream effectors, thus transducing signals from GPCR (4–6). Because Gα has intrinsic GTPase activity, the Gα subunit subsequently returns to the Gα·GDP form, which marks the termination of the GPCR signaling. Many proteins have been discovered as regulators of the GTP- and GDP-bound forms of the Gα reaction cycle. Among these, GoLoco motif proteins were discovered to bind specifically to GDP-loaded Gα$_i$ or Gα$_o$ and inhibit the spontaneous release of GDP from Gα. These GoLoco proteins are referred to as guanine nucleotide dissociation inhibitors (GDIs) (7–11).

The GoLoco motif (8, 12, 13) was first identified as a conserved sequence of 19 amino acids, occurring singly or as tandem repeats in a variety of signaling proteins across the animal kingdom (7). Our understanding of the molecular mechanism of the GDI function of GoLoco proteins is mainly based on the crystal structure of RGS14 GoLoco bound to Gα$_{i1}$·GDP (14), which shows that the conserved GoLoco motif and its variable C-terminal tail interact with the Ras-like and all-helical domains of Gα$_{i1}$, respectively. A so-called "arginine finger" formed by the highly conserved (D/E)QR triad in the conserved GoLoco motif extends into the GDP-binding pocket and directly contacts the α- and β-phosphates of GDP (14). This structure and the subsequent mutagenesis and structural studies (14–18) suggested an appealing hypothesis: the highly variable C-terminal sequences following the conserved GoLoco motifs and the all-helical domain of Gα subunits are likely the specificity determinants of interactions between GoLoco motifs and different Gα subunits. However, because there no structures of GoLoco motifs in complex with Gα other than the

---

[1] These authors contributed equally to this work.

[2] Senior Fellow of the Institute for Advanced Study, HKUST. To whom correspondence may be addressed: Div. of Life Science, Hong Kong University of Science and Technology, Clear Water Bay, Kowloon, Hong Kong, China. Tel.: 852-23588709; E-mail: mzhang@ust.hk.

[3] To whom correspondence may be addressed: Shanghai Key Laboratory of Molecular Catalysis and Innovative Materials, Dept. of Chemistry and Institute of Biomedical Sciences, 220 Handan Rd., Shanghai 200433, China. Tel.: 86-21-65643985; Fax: 86-21-65641740; E-mail: wnwang@fudan.edu.cn.

[4] The abbreviations used are: GPCR, G protein-coupled receptor; GL, GoLoco; GDI, guanine nucleotide dissociation inhibitor; TPR, tetratricopeptide; aa, amino acids; ITC, isothermal titration calorimetry.

$G\alpha_{i1}$·RGS14 complex are available to date, the above hypothesis remains untested.

LGN is a multidomain scaffolding protein containing eight tetratricopeptide (TPR) repeats in its N-terminal region, a flexible linker sequence in the middle, and four GoLoco motifs in the C-terminal end (19, 20). LGN is an evolutionarily conserved protein (Pins in *Drosophila*, and GPR1/2 in *Caenorhabditis elegans*) that plays crucial roles in regulating spindle orientations during asymmetric cell division (19, 21) and can be considered as an example member of the multiple GoLoco motif protein family. It forms a ternary protein complex with nuclear mitotic apparatus protein NuMA (Mud in *Drosophila* and Lin5 in *C. elegans*) and cortical membrane-bound $G\alpha_{i/o}$ via its TPR repeats and GoLoco motifs, respectively (22–28). The central linker of LGN binds to the guanylate kinase domain of the DLG family scaffold protein in a phosphorylation-dependent manner (29–31). In *Drosophila* neuroblast, loss of Pins or $G\alpha_i$ affects cell polarity as well as mitotic spindle orientation (32). In mammals, overexpression or removal of LGN results in dramatic spindle rocking in metaphase and improper spindle pole organization (19, 21, 33). The binding of $G\alpha_i$ through the GoLoco motifs was shown to regulate the cortical localization of LGN (33). Thus, the LGN GoLoco motifs can be viewed as scaffolding modules in tethering the TPR repeat partners (*e.g.* NuMA/Mud and mInsc/Insc) of LGN to the cell cortex via binding to membrane-attached $G\alpha_i$. Interestingly, the GoLoco motifs of LGN can directly bind to TPR repeats intramolecularly, thus keeping LGN in an autoinhibited conformation (22). $G\alpha_i$·GDP binding to GoLoco motifs releases the autoinhibited conformation of LGN and renders LGN TPR repeats capable of binding to NuMA (22, 34), although the mechanistic basis of the LGN autoinhibition is unknown.

In this study, we performed detailed biochemical and structural analyses of the interactions between LGN GoLoco motifs and $G\alpha_i$·GDP. We demonstrate that in contrast to the RGS14/$G\alpha_i$·GDP interaction, only a few residues of the highly variable sequences C-terminal to the conserved GoLoco motifs of LGN are involved in binding to $G\alpha_i$·GDP. The structures of two LGN GoLoco motifs in complex with $G\alpha_i$ reveal a double Arg finger sequence (RΨ(D/E)(D/E)QR) within the GoLoco motif that is specifically involved in the GDP coordination. We further show that the LGN GoLoco·$G\alpha_i$·GDP interaction observed in this study likely represents a general mode of GoLoco motif-mediated $G\alpha$ binding. We further demonstrate that the LGN GoLoco motifs are potent GDIs. Thus, the LGN GoLoco motifs can function as a $G\alpha$/LGN/NuMA/Insc scaffold as well as a regulator of $G\alpha$ signaling in asymmetric cell division.

EXPERIMENTAL PROCEDURES

Protein Expression and Purification—The human $G\alpha_{i3}$, $G\alpha_{i1}$, mouse LGN GL fragments were individually cloned into a modified version of pET32a vector. All the mutations were created using the standard PCR-based method and confirmed by DNA sequencing. Recombinant proteins were expressed in *Escherichia coli* BL21 (DE3) host cells at 16 or 37 °C and were purified by using a Ni^{2+}-nitrilotriacetic acid-agarose affinity chromatography followed by size exclusion chromatography. For *in vitro* biochemical analysis, LGN GLs were expressed as the GST-fused proteins and purified by GSH-Sepharose affinity chromatography.

Isothermal Titration Calorimetry Measurements—ITC measurements were performed on an ITC200 Micro calorimeter (MicroCal) at 25 °C. All protein samples were dissolved in the buffer containing 50 mM Tris, pH 8.0, 100 mM NaCl, and 1 mM EDTA. The titrations were carried out by injecting 40 μl of $G\alpha_{i3}$·GDP aliquots (0.2 mM) into LGN GLs fragments fused to the C-terminal end of thioredoxin (0.02 mM) at time intervals of 2 min to ensure that the titration peak returned to the base line. The titration data were analyzed using the program Origin7.0 from MicroCal.

Fluorescence Polarization Assay—Fluorescence polarization assay were performed on a PerkinElmer LS-55 fluorimeter equipped with an automated polarizer at 25 °C. Commercial synthesized peptides were labeled with fluorescein 5-isothiocyanate (Invitrogen) at the N termini. In a typical assay, the FITC-labeled peptide (~1 μM) was titrated with binding partners in a 50 mM Tris pH 8.0 buffer containing 100 mM NaCl, 1 mM DTT, and 1 mM EDTA. The K_D values were obtained by fitting the titration curves with the classical one-site binding model, with or without invoking the Hill coefficient model.

GST Pulldown Assay—For GST pulldown assay, GST or GST-tagged proteins (60 μl from 1 mg/ml stock solutions) were first loaded to 40 ml GSH-Sepharose 4B slurry beads in an assay buffer (50 mM Tris, pH 8.0, 100 mM NaCl, 1 mM DTT, and 1 mM EDTA). The GST fusion protein-loaded beads were then mixed with potential binding partners, and the mixtures were incubated for 1 h at 4 °C. After three times washing, proteins captured by affinity beads were eluted by boiling, resolved by 15% SDS-PAGE, and detected by Coomassie Blue staining.

Analytical Gel Filtration Chromatography—Analytical gel filtration studies were carried out on an AKTA FPLC system (GE Healthcare). Proteins at concentration of 10–20 μM in a volume of 100 μl were loaded on a Superose 12 10/300 GL column 20 (GE Healthcare) equilibrated with the buffer containing 50 mM Tris, pH 8.0, 100 mM NaCl, 1 mM DTT, and 1 mM EDTA. Protein elution was detected by absorbance at 280 nm.

GDI Activity Assay—Measurements of AlF_4^--induced increase of intrinsic tryptophan fluorescence were performed on the PerkinElmer LS-55 spectrometer with excitation at 292 nm and emission at 342 nm. Purified $G\alpha_{i3}$ protein was diluted in 2-ml cuvettes to 200 nM in a preactivation buffer (100 mM NaCl, 100 μM EDTA, 2 mM $MgCl_2$, 20 μM GDP, 20 mM Tris-HCl, pH 8.0) and incubated at 30 °C. At the time points 400 and 500 s after $G\alpha_{i3}$ dilution, 2 mM NaF and 30 μM $AlCl_3$ (final concentrations), respectively, were added to the reaction mixture, and fluorescence intensity changes as a function of time were recorded. The GDI activities of GL peptides were assayed by repeating the above procedure except that the reaction mixtures contained defined concentrations of specific peptides.

The measurements of GTPγS binding were also performed on PerkinElmer LS-55 spectrometer with excitation at 485 nm and emission at 530 nm (slit widths each at 2.5 nm). BODIPY FL-GTPγS was diluted to 1 μM in buffer (20 mM Tris-HCl, pH 8.0, 1 mM EDTA, and 10 mM $MgCl_2$) and equilibrated to 30 °C in 2-ml cuvettes. Purified $G\alpha_{i3}$ was diluted to 100 nM in the buffer (100 mM NaCl, 100 μM EDTA, 2 mM $MgCl_2$, 20 μM GDP, 20 mM

TABLE 1

Statistics of x-ray crystallographic data collection and model refinement

The numbers in parentheses represent the value for the highest resolution shell.

Data sets	Gα$_{i3}^{QtoL}$_GL4	Gα$_{i1}$_GL4	Gα$_{i3}$_GL4	Gα$_{i3}$_GL3
Space group	P6$_1$22	P6$_1$22	P6$_1$22	P6$_1$22
Unit cell (Å)	$a = 207.3$, $c = 236.6$	$a = 207.4$, $c = 236.7$	$a = 209.6$, $c = 237.2$	$a = 209.7$, $c = 235.5$
No. of unique reflections	66,825	66,971	39,388	35,265
Resolution limit (Å)	50.00–2.90 (2.95–2.90)	50.00–2.90 (2.95–2.90)	50.00–3.50 (3.56–3.50)	50.00–3.60 (3.66–3.60)
Redundancy	10.8 (11.2)	9.4 (9.7)	4.4 (4.5)	9.2 (9.4)
Completeness (%)	100 (100)	100 (100)	98.8 (99.9)	99.7 (100)
I/σ_I	27.5 (3.6)	25.1 (3.3)	14.7 (1.8)	37.6 (5.8)
R_{merge} (%)[a]	9.8 (76.2)	9.6 (73.5)	11.0 (75.7)	7.3 (39.6)
Structure refinement				
Resolution range (Å)	43.04–2.90 (3.00–2.90)	47.69–2.90 (3.00–2.90)	49.65–3.50 (3.61–3.48)	39.63–3.62 (3.75–3.62)
R_{cryst}/R_{free} (%)[b]	22.0/25.0 (32.6/42.4)	22.0/24.5 (31.9/36.1)	22.6/26.1 (30.1/35.8)	22.8/25.3 (27.7/31.0)
Root mean square deviation bonds (Å)/angle (°)	0.010/1.36	0.010/1.41	0.011/1.63	0.009/1.26
Average B factor (Å^2)[c]	67.90	66.50	106.40	123.50
No. of atoms				
Protein atoms	10907	10921	10601	10141
Water molecules	12	35	0	0
Ligands	25	25	11	11
No. of reflections				
Working set	63256 (6246)	63457 (6234)	37222 (3584)	33318 (3272)
Test set	3375 (313)	3385 (343)	1963 (195)	1754 (151)
Ramachandran plot[c]				
Favored (%)	95.5	95.8	92.2	90.1
Allowed (%)	4.5	4.2	7.4	8.2
Outliers (%)	0	0	0.4	1.7

[a] $R_{merge} = \Sigma|I_i - <I>|/\Sigma I_i$, where I_i is the intensity of measured reflection, and $<I>$ is the mean intensity of all symmetry-related reflections.
[b] $R_{cryst} = \Sigma||F_{calc}| - |F_{obs}||/\Sigma F_{obs}$, where F_{obs} and F_{calc} are observed and calculated structure factors. $R_{free} = \Sigma_T||F_{calc}| - |F_{obs}||/\Sigma F_{obs}$, where T is a test data set of ~5% of the total unique reflections randomly chosen and set aside prior to refinement.
[c] B factors and Ramachandran plot statistics are calculated using MOLPROBITY (45).

Tris-HCl, pH 8.0) and preincubated with GL peptides (with different concentrations) at 30 °C for 10 min before addition to the cuvette. Relative fluorescence levels were set to 0 at the average fluorescence reading over the first 70 s, and Gα$_{i3}$/GL mixtures were added at the time point of 100 s.

Crystallography—Crystals of the Gα$_{i1(3)}$ in complex with GL3/4 (diluted to 7.5 mg/ml in 50 mM Tris, pH 8.0, 100 mM NaCl, 1 mM EDTA, 1 mM DTT, 10 mM Mg^{2+}, 20 μM GDP buffer) were obtained by the hanging drop vapor diffusion method at 18 °C. The crystals were grown in buffer containing 0.5 M ammonium sulfate, 1.0 M lithium sulfate monohydrate, 0.1 M sodium citrate tribasic dehydrate, pH 5.6. Crystals were soaked in crystallization solution containing a higher concentration (1.5 M) of lithium sulfate for cryo-protection. All the diffraction data were collected at Shanghai Synchrontron Radiation Facility BL17U at a wavelength of 0.9793 Å using a single crystal of each complex. The diffraction data were processed and scaled using HKL2000 (35). Molecular replacement was used to solve the structure of Gα$_{i1(3)}$·GL4(3) with the program Molrep (36). The crystal structure of RGS14·Gα$_{i1}$ complex (Protein Data Bank code 1KJY) was used as a search model by removing the RGS14 peptide. The initial model was rebuilt manually and then refined using REFMAC (37) and PHENIX (38) against the whole data set. Further manual model building and adjustment were completed using COOT (39). The final refinement statistics are summarized in Table 1.

RESULTS

Mapping the Minimal Gα$_i$·GDP Binding Sequences in LGN GoLoco Motifs—The C-terminal region of LGN contains four GoLoco motifs, each of which consists of a conserved 19-residue fragment followed by a stretch of variable amino acid residues with different lengths (Fig. 1A). We define the full-length GoLoco motif to be the conserved 19-residue fragment plus all of the following C-terminal sequence before the start of the next GoLoco motif core. With this definition, each GL1, 2, 3, and 4 motif of LGN consists of 54, 51, 34, and 51 residues, respectively (Fig. 1A). Previous structural study of the Gα$_{i1}$·RGS14-GoLoco complex showed that the 16-residue sequence C-terminal to the GoLoco core motif make extensive contacts with Gα$_{i1}$ and thus are essential for the interaction between Gα$_{i1}$ and RGS14 (14). To understand the interaction between LGN and Gα$_i$, we set out to map the minimal Gα$_i$·GDP binding sequence of each LGN GL. We first used GST-fused LGN GL with different lengths to pull down purified Gα$_{i3}$·GDP in our binding assay. This assay showed that each GL containing only the 19-residue core displayed only a background level of binding to Gα$_{i3}$·GDP (Fig. 1B). Obvious binding of Gα$_{i3}$·GDP to GL1 and GL4 was observed by extending the conserved 19-residue GL core by two residues (Fig. 1B). Any one of LGN GLs with length equal to or longer than 25 residues displayed comparable binding to their corresponding full-length motifs (Fig. 1B). We next measured the quantitative binding affinities of each of the four GLs to Gα$_{i3}$·GDP using isothermal titration calorimetry or fluorescence spectroscopy. Such quantitative binding assays revealed that the four full-length GLs share similar affinities ($K_D = 54$–96 nM) in binding to Gα$_{i3}$·GDP (Fig. 1C). In agreement with the results derived from the pulldown binding assay, each LGN GL with a length of 25 residues has an essentially same binding affinity compared with the corresponding full-length motif (Fig. 1C), indicating that each of the 25-residue LGN GL contains the complete Gα$_i$·GDP binding sequence. This finding is in sharp contrast to the interaction
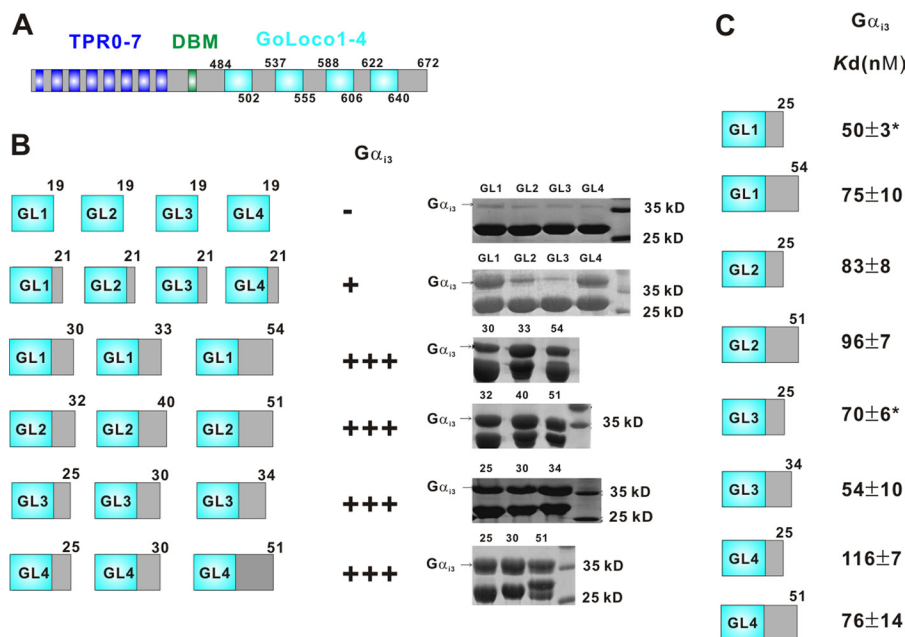
FIGURE 1. **Characterization of the binding between Gαᵢ·GDP and the four LGN GLs.** *A*, schematic diagram of the domain organization of LGN. *DBM* denotes the DLG-binding domain of LGN. *B*, GST pulldown assay of the binding between LGN GLs with variable lengths (indicated by the *number* at the *top* of each GL) with Gαᵢ₃·GDP. *C*, ITC and fluorescence-based (denoted with *asterisks*) measurements of the binding affinities of Gαᵢ₃·GDP with LGN GLs of different lengths.

between Gαᵢ·GDP and the RGS14 GoLoco motif, which requires a total length of 35 residues (14). Consistent with earlier studies (40), the LGN GLs bind to Gαᵢ₃·GTPγS with a ~100-fold weaker affinity than to Gαᵢ₃·GDP (data not shown).

Gαᵢ·GDP Can Simultaneously Bind to All Four LGN GLs— We next asked whether Gαᵢ·GDP can simultaneously bind to the multiple GLs of LGN. We first tested the interaction between Gαᵢ·GDP and the LGN GL34 tandem (aa 587–650), because the intervening sequence between the core sequences of GL3&4 is the shortest (15 residues to be exact; Fig. 1*A*). According to the structure of Gαᵢ₁·RGS14 complex (14), two successive GL core sequences separated by a 15-residue linker cannot bind to two Gαᵢ because the bound Gαᵢ molecules would crash into each other. We examined the binding stoichiometry between LGN-GL34 and Gαᵢ₃·GDP using analytical gel filtration chromatography. Upon addition of 2 or 3 molar ratios of Gαᵢ₃ to GL34, a peak corresponding to a (Gαᵢ₃·GDP)₂·GL34 complex was detected (Fig. 2*A*), indicating that the two GLs in GL34 can simultaneously bind to Gαᵢ₃·GDP. To further substantiate that the elution peak at ~11.60 ml in Fig. 2*A* represents the 2:1 stoichiometric complex formed between Gαᵢ₃·GDP and GL34, we used two GL34 mutants (L594E and I628E), in which either the Gαᵢ₃·GDP binding site on GL3 (the L594E mutant) or on GL4 (the I628E mutant) was disrupted. On the gel filtration column, the 1:2 mixtures of the two GL34 mutants with Gαᵢ₃·GDP were eluted at a volume significantly larger than the wild type GL34, and a large portion of free Gαᵢ₃·GDP was also detected (Fig. 2*B*); presumably the GL34 mutants only formed 1:1 stoichiometric complex with Gαᵢ₃·GDP. This result also confirms that the wild type GL34 can form a 1:2 stoichiometric complex with Gαᵢ₃·GDP. Further lengthening of the linker between GL3 and GL4 by inserting 10 flexible residues (five GS repeats, referred to as GL34Ins5GS)

did not alter the elution profile of its complex with Gαᵢ₃·GDP (data not shown), indicating that the 15-residue intervening sequence between GL3 and GL4 is sufficiently long for two molecules of Gαᵢ₃·GDP to bind simultaneously to GL34. Similarly, two molecules of Gαᵢ₃·GDP are capable of binding to LGN-GL12 (aa 483–586) or GL23 (aa 537–620). (Fig. 2, *C* and *D*). Additionally, three molecules of Gαᵢ₃·GDP were found to bind simultaneously to GL123 (aa 483–620) or GL234 (aa 537–650) of LGN (Fig. 2, *E* and *F*).

To characterize the binding stoichiometry more precisely, ITC analyses were performed. The titration profiles of Gαᵢ₃·GDP to GL23 and GL34 can be well fitted with the model using one set of identical sites, yielding overall stoichiometries of 1.9:1 and 1.8:1, respectively (Fig. 3, *A* and *B*, and Table 2), consistent with the binding stoichiometry derived from the gel filtration analyses. The apparent binding affinity of GL23 was similar to those of the individual GoLocos, whereas GL34 had a weaker binding affinity than that of GL3 or GL4 (Table 2 and Fig. 1*C*). The titration profile of Gαᵢ₃·GDP to the triple-GoLoco-containing protein GL234 was also fitted with the model with one set of binding sites, giving a weaker binding affinity of ~358 nM and a binding stoichiometry of 3.1:1 (Fig. 3*C* and Table 2). The purified GL234 protein underwent slight degradation, which might affect the accuracy of the binding affinity measurement. The titration profile of Gαᵢ₃·GDP to GL12, however, was best fitted with the model that assumes two sets of binding sites (Fig. 3*D*), yielding one strong site (K_D = ~11 nM) and one weak site (K_D = ~188 nM) (Table 2). The ITC titration profile of Gαᵢ₃·GDP to GL123 was also fitted with the 'two sets of binding sites' model, giving rise to two strong sites (K_D ~ 4 nM) and one weak site (K_D ~ 186 nM) (Fig. 3*E* and Table 2). Similar atypical profiles of ITC titrations were also observed in the analyses of AGS3-GLs/Gαᵢ·GDP interaction (41). It is worth
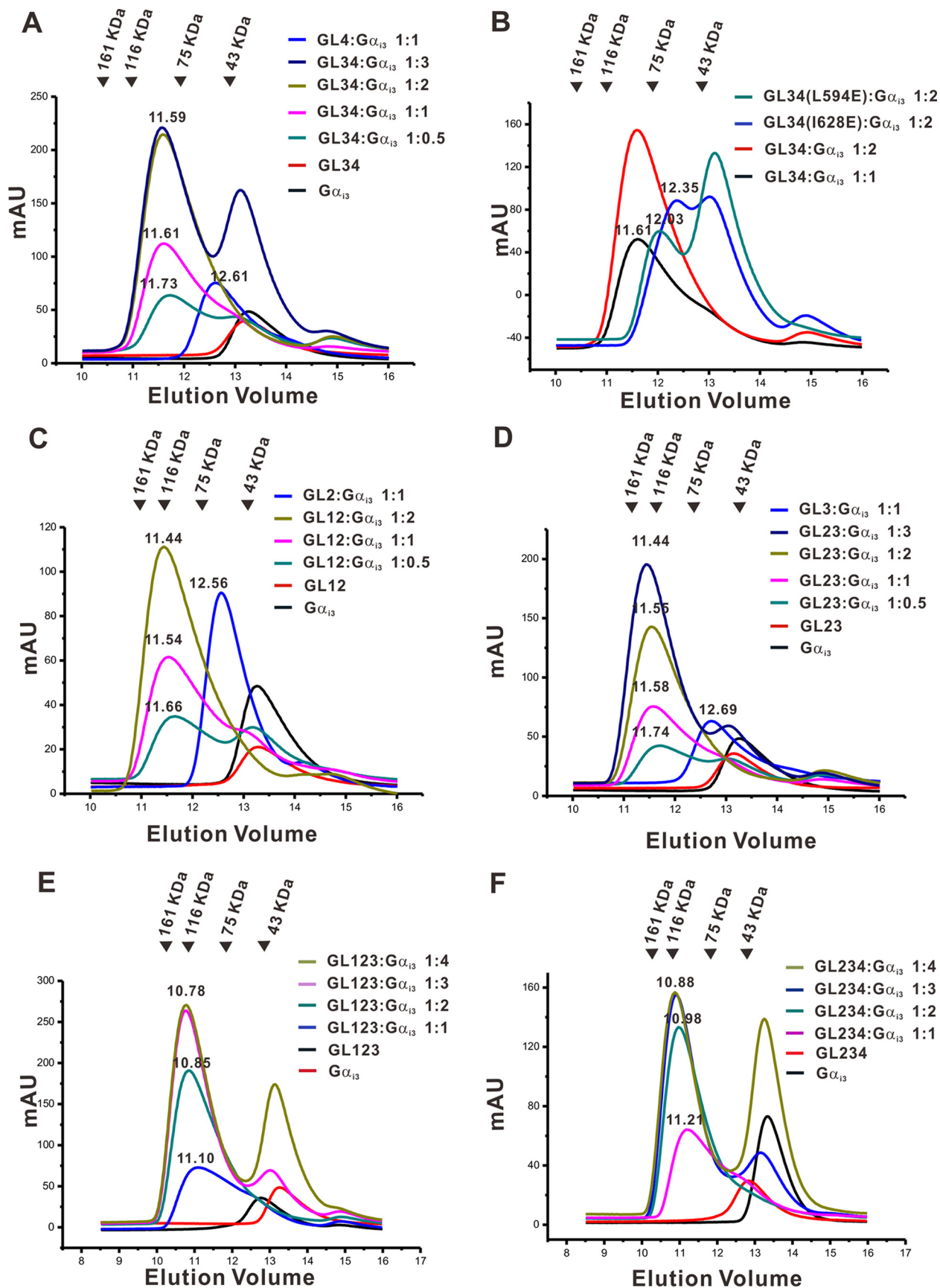
FIGURE 2. **Gα$_i$·GDP binding to multiple GL containing fragments of LGN analyzed by analytical gel filtration chromatography.** *A*, the binding of LGN-GL34 to different molar ratios of Gα$_{i3}$·GDP. *B*, the binding of LGN-GL34(L594E) and LGN-GL34(I628E) to Gα$_{i3}$·GDP. *C*, the binding of LGN-GL12 to Gα$_{i3}$·GDP. *D*, the binding of LGN-GL23 to Gα$_{i3}$·GDP. *E*, the binding of LGN-GL123 to Gα$_{i3}$·GDP. *F*, the binding of LGN-GL234 to Gα$_{i3}$·GDP.
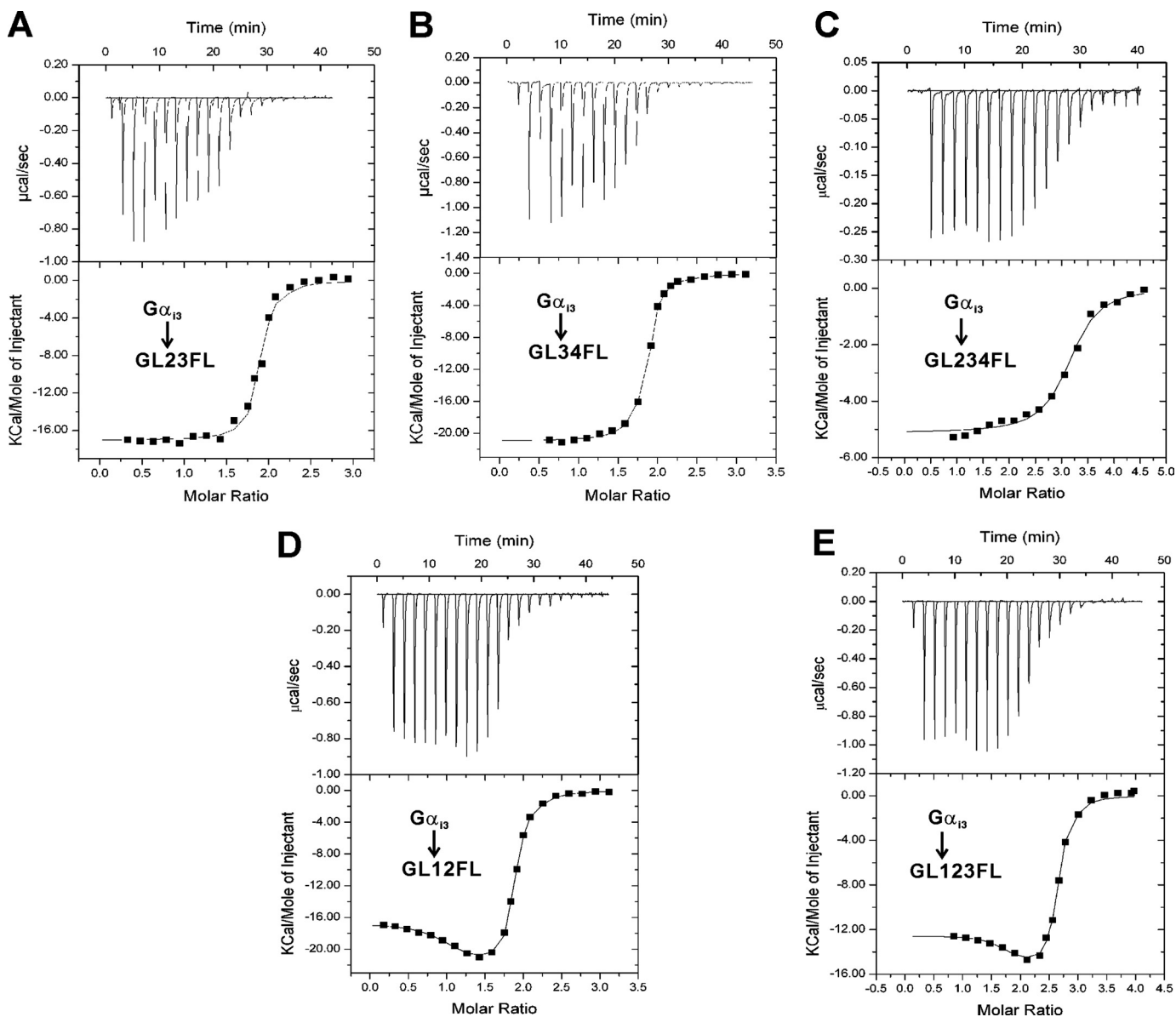
FIGURE 3. **ITC analyses of the binding of tandem GoLoco motifs to Gα$_{i3}$·GDP.** ITC measurements of binding of Gα$_{i3}$·GDP to LGN-GL23 (*A*), LGN-GL34 (*B*), LGN-GL24 (*C*), LGN-GL12 (*D*), and LGN-GL13 (*E*). The titration data were fitted with the models with one set of binding sites and two sets of binding sites. The derived thermodynamic parameters are shown in Table 2.

noting that these data analyses do not represent the complete description of the thermodynamics of the interactions between tandem LGN-GoLoco repeats and Gα$_{i3}$·GDP, in which intersite cooperativity likely exists. Because the full-length GoLoco region of LGN, *i.e.*, GL1234, suffers from severe degradation, we did not analyze the binding property of GL1234 directly. However, the ITC titration data, consistent with the gel filtration analyses, strongly suggested that the full-length LGN binds Gα$_{i3}$·GDP with a stoichiometry of 1:4. The four GoLoco motifs of LGN have intrinsically similar binding affinities to Gα$_{i3}$·GDP. To explore the molecular details of the binding, we proceeded to determine the crystal structure of the Gα$_i$·LGN-GoLoco complex.

Overall Crystal Structures of GL3 and GL4 in Complex with Gα$_i$·GDP—Extensive efforts have been put to screen various constructs of the four LGN GLs in complex with GDP-loaded

Gα$_{i3}$ or Gα$_{i1}$, and we succeeded in obtaining well diffracting crystals for synthetic GL4 ([621]DEDFFSLILRSQAKRMDEQRV-LLQRD[645]) and GL3 ([587]DEDFFDILVKCQGSRLDDQRCA-PPS[611]) peptides in complex with Gα$_{i1/3}$·GDP. The Gα$_{i1}$·GL4, Gα$_{i3}$·GL4, and Gα$_{i3}$·GL3 complexes diffracted to 2.9, 3.5, and 3.6 Å resolutions, respectively (Table 1). According to a previous structure-based protein design study, point mutations on Gα$_i$ (E116L, Q147L, and E245L, respectively) can enhance its binding affinity to various GLs (15). We therefore constructed such three Gα$_{i3}$ mutants, hoping that the mutants might have higher affinities in binding to LGN GLs and thus yield better quality complex crystals. Opposite to our expectation, none of these mutants showed obviously enhanced binding to LGN GLs (data not shown). Nonetheless, the Q147L-Gα$_{i3}$ mutant·GL4 complex yielded better diffracting crystals (2.9 Å) than the wild type Gα$_{i3}$·GL4 complex.

TABLE 2

Thermodynamic parameters of the bindings of LGN GoLoco motifs to Gα$_{i3}$·GDP determined by ITC titration

The titration data of GL12 and GL123 were fitted with the two sets of binding sites model, whereas the other data were fitted with the one set of binding sites model. *N* denotes the number of binding sites in each model.

	N	K_D	ΔH	ΔS	ΔG
		n$_M$	*kcal mol^{-1}*	*cal mol^{-1} K^{-1}*	*kcal mol^{-1}*
GL12					
Site 1	0.97	11.27	−16.69	−18.7	−11.12
Site 2	0.89	188.32	−22.80	−44.4	−9.57
GL123					
Site 1	1.63	4.69	−12.55	−3.97	−11.37
Site 2	1.0	186.22	−15.46	−21.0	−9.20
GL23	1.86	87.72	−17.05	−24.0	−9.90
GL34	1.81	173.61	−20.97	−37.2	−9.88
GL234	3.08	358.42	−5.12	11.9	−8.67

The structures of Gα$_{i1(3)}$·GL4 and Gα$_{i3}$·GL3 were solved by molecular replacement using the Gα$_{i1}$·RGS14 structure as the search model (Protein Data Bank code 1KJY) (14). The Gα$_i$·GDP structure is well defined, and 21–22 amino acids of the GL3 or GL4 peptide are ordered in the structures of complexes (Fig. 4, *A* and *B*). The structures of Gα$_i$ in the Gα$_{i1(3)}$·GL4 and Gα$_{i3}$·GL3 complexes are highly similar to that in the Gα$_{i1}$·RGS14 complex (root mean square deviation of 0.67 Å), except for the Switch II region, which is shifted further away from the LGN-GL peptides because of the presence of two bulky hydrophobic residues in the GL peptides (Fig. 5, *A* and *B*). The GL peptides in the three complexes adopt highly similar structures (Fig. 4*C*). The N-terminal 10 residues of each LGN GL peptide (aa 623–632 of GL4 and aa 589–598 of GL3), which corresponds to the first half of the conserved 19-residue GL core, forms an α-helix that occupies the cleft between Switch II and α3 of Gα$_i$ (Fig. 4*A*). The following eight residues of the GL core (aa 633–640 of GL4 and aa 599–606 of GL3) forms a "lid" in covering GDP. Only three or four residues C-terminal to the GL core (aa 641–643 of GL4 and aa 607–610 of GL3) were found to bind to the all-helical domain of Gα$_i$ (Fig. 4). The structures of the LGN GL peptides in complex with Gα$_i$ are entirely consistent with our biochemical data, showing that extending of the conserved GL core at the C-terminal end by three or four residues is necessary and sufficient for LGN GLs to bind to Gα$_i$ (Figs. 1 and 2). The structures of the complexes also indicate that LGN GLs should function as GDIs by directly stabilizing the bound GDP as well as the interaction between the Ras-like domain and the all-helical domain of Gα$_i$ (Fig. 4*A*).

A General Interaction Mode Revealed by the LGN GLs in Complex with Gα$_i$—Although the structures of Gα$_i$ bound to the GLs of RGS14 and LGN are highly similar, the conformation of Gα$_i$-bound GLs of RGS14 and LGN are distinctly different (Fig. 5). First, a 16-residue fragment C-terminal to the conserved GL core of RGS14 is required for binding to Gα$_i$, and this 16-residue fragment forms ordered structure and has extensive interactions with the all-helical domain of Gα$_{i1}$ (14). In LGN-GL4/GL3, in contrast, only three or four residues C-terminal to the GL core are required for binding to Gα$_i$ (Fig. 4*A*). Second, the orientation of the variable C-terminal tail of the RGS14 GL peptide is opposite to that of the LGN GL peptides (Fig. 5*A*). In the LGN GL4·Gα$_i$ complex, the hydrophobic side chains of Val[641], Leu[642], and Leu[643] interact with Val[72] and Tyr[69] from
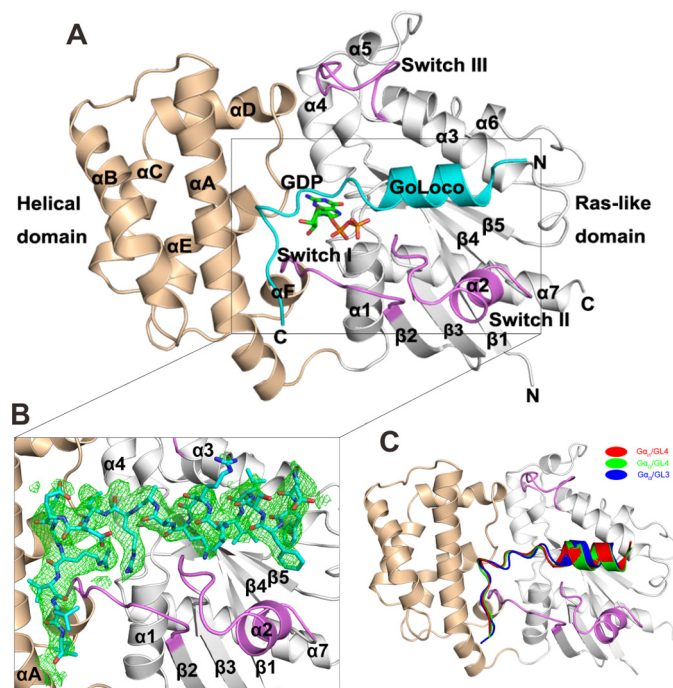

FIGURE 4. **Crystal structures of Gα$_{i3}$ in complex with GL4 and GL3, respectively.** *A*, ribbon diagram showing the crystal structure of LGN-GL4 in complex with Gα$_{i1}$·GDP. GDP is shown in the ball-and-stick model. All-helical domain and Ras-like domain of Gα$_{i1}$ is shown in *wheat* and *light gray*, respectively. The three switches are shown in *violet*, and the GL4 peptide is shown in *cyan*. *B*, the $F_o − F_c$ density map of GL4 peptide is shown in *green* and contoured at 3.0 σ. *C*, comparison of the structures of the Gα$_{i1}$·GL4, Gα$_{i3}$·GL4, and Gα$_{i3}$·GL3 complexes by superimposing the backbone atoms in the three structures. Gα$_{i1}$ is shown the same as in *A*, whereas Gα$_{i3}$ in complex with GL3 (root mean square deviation of 0.76 Å) and GL4 (root mean square deviation of 0.51 Å) is not shown. GL3 peptide is shown in *blue*, and GL4 peptides bound to Gα$_{i1}$ and Gα$_{i3}$ are shown in *red* and *green*, respectively.

the αA helix of the Gα$_i$ all-helical domain; thus the C-terminal end of GL4 extends toward the N-terminal end of Gα$_i$ αA (Fig. 5*C*). The residue corresponding to Val[641] in the RGS14 peptide is Gly[517] (Fig. 5*D* and Fig. 6*A*). The backbone carbonyl oxygen of Gly[517] forms two hydrogen bonds with side chains of Ser[75] and Gln[79] from Gα$_i$ αA. The unique backbone dihedral angles ($\phi = 78°$, $\psi = -171°$) of Gly[517], which are not allowed by other amino acids, enable the C-terminal tail of the RGS14 GL peptide to take a sharp turn at this position and extend to the C-terminal end of Gα$_i$ αA (Fig. 5, *A* and *D*). Sequence alignment of all known GLs from mammals reveals that only the GLs of RGS14 and RGS12 contain a Gly right after the conserved core motif, and the C-terminal residues of these two GLs share the identical sequence (Fig. 6*A*). The above structure-based amino acid sequence analysis suggests that the LGN GL/Gα$_i$ interactions observed in this study represent the general mode of the interactions between GoLoco proteins and Gα$_i$. RGS14 and RGS12, instead, may represent a special subclass of GoLoco proteins in terms of Gα$_i$ binding.

The Double Arg Finger-mediated GDP Binding of LGN GLs— The structure of the Gα$_{i1}$·RGS14 GL complex shows that a highly conserved (D/E)QR triad at the C-terminal end of the conserved GL core plays a critical role in binding to Mg^{2+}-GDP (14). Similar to the Gα$_{i1}$·RGS14 GL interaction, the side chain of Arg[640] (Arg[606]) of GL4 (GL3) in the (D/E)QR triad, which is equivalent to Arg[516] of RGS14, is inserted into the GDP-bind-
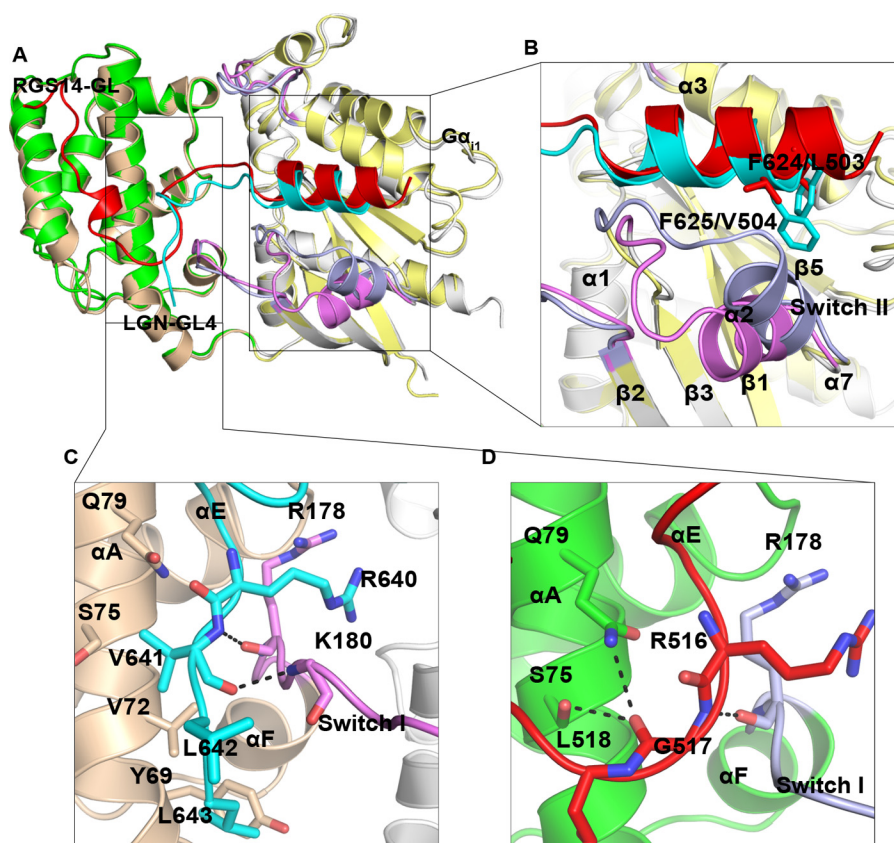
FIGURE 5. **Comparison of the crystal structures of Gα_{i1}·GL4 and Gα_{i1}·RGS14 complexes.** *A*, comparison of the crystal structure of Gα_{i1}·GL4 (*cyan*) with that of Gα_{i1}·RGS14 (*green*). The all-helical domain and Ras-like domain of Gα_{i1} are colored *wheat* and *light gray*, respectively. The Switch I, II, and III regions of Gα_{i1} in complex with LGN-GL4 and with RGS14 are highlighted with *violet* and *light blue*, respectively. *B*, comparison of the structural details of the α-helical region of LGN-GL4 and RGS14-GL, showing that the larger hydrophobic side chains of LGN-GL4 result in the shift of the Switch II of Gα_{i1}. *C*, structure details of the C terminus of LGN-GL4, showing that two backbone hydrogen bonds stabilize the C-terminal conformation. *D*, structure details of the sharp turn at Gly[517] of RGS14 peptide. Hydrogen bonds formed between RGS14 and Gα_{i1} are shown with *dashed lines*.

ing pocket and binds to α-phosphate of GDP (Fig. 6*B*). However, there is a distinct feature of GL4/GL3 in GDP binding with respect to RGS14 GL. Another highly conserved Arg five residues upstream of the Arg in the (D/E)QR triad in LGN GL peptides (Arg[635] in GL4 and Arg[601] in GL3) binds to the α and β phosphates of GDP (Fig. 6*B*). In RGS14 GL, the residue corresponding to this second Arg is a Gly, and a Mg^{2+} ion was found to be necessary to stabilize the β phosphates of GDP (14). Therefore, different from RGS14, LGN GLs use two Arg residues instead of one to bind to and stabilize GDP. The structures of the LGN GLs in complex with Gα_i further indicate that the LGN GLs can bind to GDP-bound Gα_i independent of the presence of Mg^{2+}. This structure-based prediction is confirmed by direct binding experiment (data not shown). Sequence alignment analysis reveals that, except for RGS14 GL, the rest of GLs all contain a (R/K)*X*(D/E)(D/E)QR GDP-binding sequence (Fig. 6*A*), and we refer to this sequence as the double Arg finger. This sequence analysis further supports that the LGN GL/Gα_i interaction represents the general mode of GL-mediated binding to Gα.

The Double-arginine Fingers Are Critical to the GDI Activities of LGN-GLs—To confirm the functional importance of the two Arg in the double-arginine finger in LGN GLs, we performed point mutations of the two arginines and tested the Gα_i·GDP binding affinities and GDI activities of these mutants. Single substitution mutations (R635G, R635A, and R640A) caused ~50-fold decrease in GL4 binding to Gα_i·GDP, and the double mutation (R635A/R640A) led to ~500-fold Gα_i·GDP binding affinity decrease (Fig. 6*C*). Similar results were also obtained from the other LGN GLs, indicating that the two conserved arginine fingers are critical for binding of Gα_i·GDP to LGN-GLs. This finding is in contrast to the RGS14 GL, in which the substitution of the Arg in the finger with Ala or Leu did not decrease the binding affinity of RGS14 to Gα_{i1}·GDP (14). Careful examination of the crystal structures of Gα_i in complex with LGN GL peptides revealed that the side chains of the two Arg residues also form hydrogen bonds with Val[179] and Thr[181] from Gα_i (Fig. 6*B*). In contrast, the side chain of Arg[516] in RGS14 GL interacts exclusively with GDP (14).

The GDI activities of LGN GLs were evaluated by AlF$_4^-$-induced increase of intrinsic tryptophan fluorescence of Gα_i and by direct binding of BODIPY-GTPγS to Gα_i. In agreement with the previous studies (40), the four GLs exhibited similar GDI activities (data not shown). Moreover, comparison of the GDI activities of GL peptides with different lengths showed that the 25-residue minimal Gα_i-binding GL fragments shown in Fig. 1 are also sufficient for their GDI activities (data not shown). Further quantification of the GDI activities using the association rate of BODIPY-GTPγS binding revealed IC$_{50}$ values of a few μM for LGN GLs, which is slightly weaker than that of
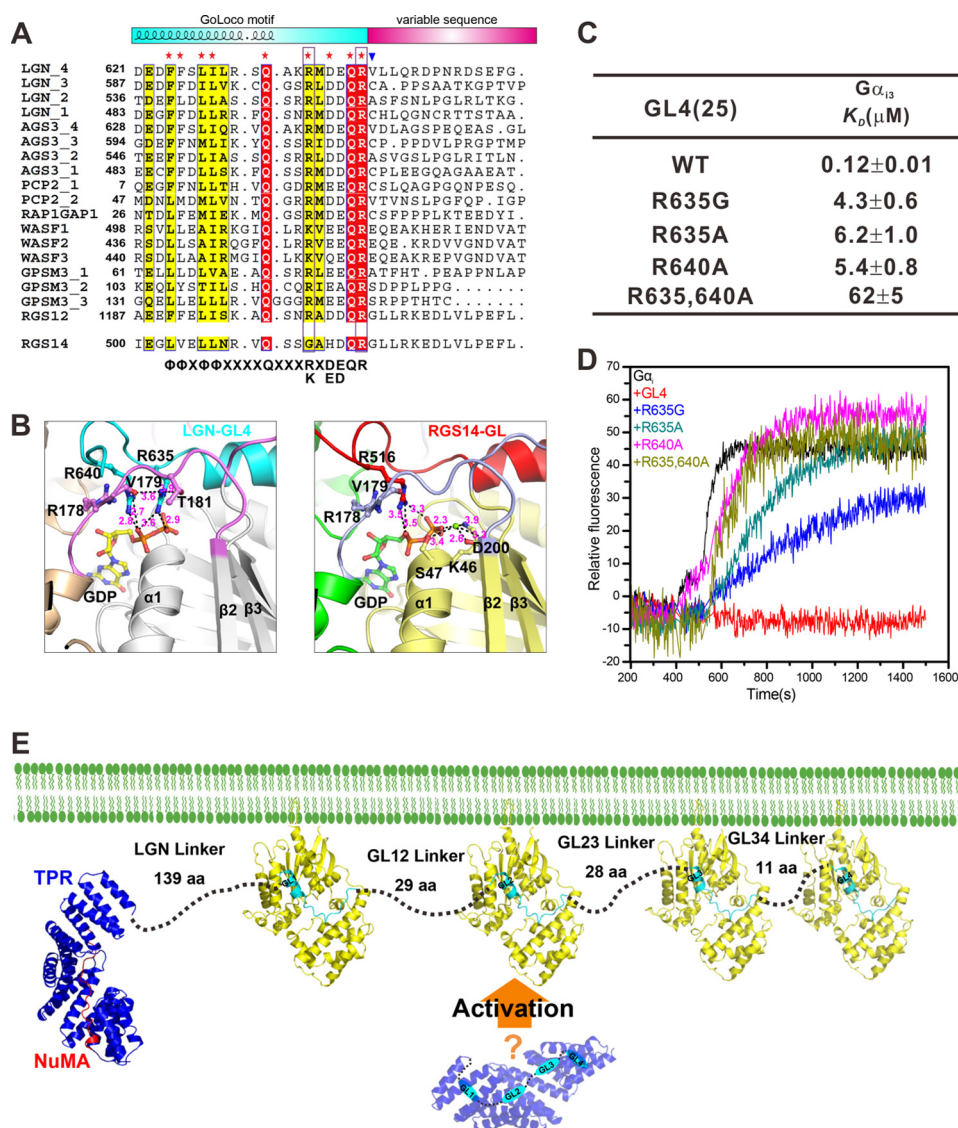
FIGURE 6. **The double arginine fingers of the LGN GLs play a crucial role in GDP coordination and GDI activity.** *A*, sequence alignment of the GLs in mammalian GoLoco proteins. Absolutely and highly conserved residues are highlighted in *red* and *yellow*, respectively. The residue right behind (D/E)QR, which determines the C-terminal direction, is highlighted with a *blue triangle*. The residues involved in the interactions with Gα$_i$ are labeled with *red stars* at the *top*. The di-arginine fingers are highlighted with *black boxes*. *B*, structural details of the GDP-binding pocket in the Gα$_{i1}$·GL4 complex and Gα$_{i1}$·RGS14 complex. Polar interactions are shown with *dashed lines*. Distances of polar interactions are shown with *magenta numbers* (Å). The color scheme is the same as in Fig. 4*A*. *C*, binding affinities of the GL4 mutants with single or double substitutions of its two arginine residues to Gα$_{i3}$·GDP derived from fluorescence-based assays. *D*, GDI activities of the wild type and mutant GL4 peptides measured with AlF$_4^-$-induced increase of intrinsic tryptophan fluorescence. *E*, structural model of the LGN·Gα$_i$·GDP complex. The TPR domain, the TPR-binding NuMA peptide, and the GLs responsible for Gα$_i$·GDP binding are shown in *blue*, *red*, and *cyan*, respectively.

RGS14 GL (data not shown). At a saturated concentration of GL peptide (GL, 200 μM; Gα$_{i3}$, 0.2 μM), the wild type LGN-GL4 showed a complete inhibition of GDP dissociation from Gα$_{i3}$ (Fig. 6*D*). The R635G-GL4 or the R635A-GL4 displayed obviously weakened GDI activities, whereas the R640A-GL4 and R635,640A-GL4 had essentially no detectable GDI activity (Fig. 6*D*). Substitution of the first Arg (Arg[601]) in the double-arginine finger of GL3 with Ala or Gly also diminished its GDI activity (data not shown). Thus, we conclude that both arginines in the double-arginine finger of LGN GoLoco motifs are important for their GDI activity.

DISCUSSION

Both the binding to GDP-loaded Gα subunits and the GDI activity of GL require residues beyond the 19-residue conserved core sequence (14, 41). Because the C-terminal flanking sequences of GLs are highly diverse among GoLoco proteins (7), it has been hypothesized that the variable C-terminal tail sequences of GLs are the specificity determinants governing GL/Gα interactions. In the present study, we demonstrate that only a few residues (3– 4 aa) C-terminal to the conserved GL core are required for LGN GLs to bind to and to inhibit GDP dissociation of Gα$_i$·GDP, a finding that is in sharp contrast to that of RGS14 GL. Sequence alignment analysis suggests that the conformation of the GL peptide in the Gα$_{i1}$·RGS14 structure is likely a unique example of GL/Gα interaction. The LGN GL/Gα$_i$ interaction described in the current study instead is likely a general binding mode between GLs and Gα. The structures of LGN GLs in complex with Gα$_i$·GDP also suggest that
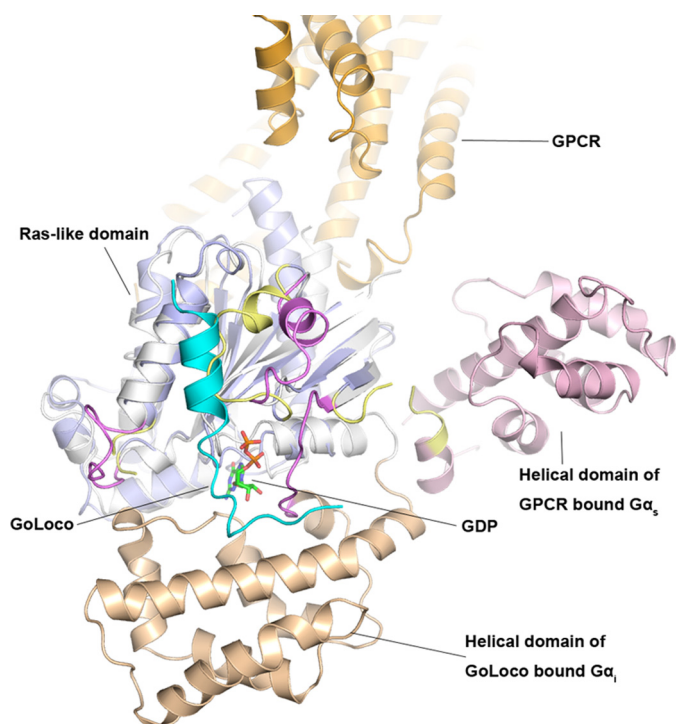
FIGURE 7. **Comparison of Gα$_{i1}$·GL4 structure with the structure of the fully activated Gα conformation derived from the β2-AR-Gαβγ structure.** The all helical domain, the Ras-like domain, and three switches of GPCR bound Gα$_s$ are shown in *light blue*, *pink*, and *yellow*, respectively. Part of the GPCR (β2-AR) is shown in *orange*. The coloring of the Gα$_{i1}$·GL4 complex is the same as in Fig. 4*A*.

the short variable C-terminal sequences of LGN GLs are unlikely to determine their binding specificity to Gα subunits. Consistently, previous studies have shown that LGN GLs bind to all three forms of GDP-loaded Gα$_i$ (i1, i2, and i3). As for the Gα$_o$·GDP binding, discrepancies exist in the literature. An early study by McCudden *et al.* (40) reported that LGN GLs selectively bind to Gα$_i$·GDP, but not to Gα$_o$·GDP or Gα$_s$·GDP. Recently, Kopein *et al.* (42) found that LGN, as well as its *Drosophila* homolog Pins, can bind robustly to both GDP-loaded Gα$_o$ and Gα$_i$.

We have demonstrated in this study that every one of the four LGN GLs can bind to Gα$_i$·GDP with high affinity. Additionally, although the LGN GL peptides are much shorter than their counterpart from RGS14, LGN GLs also act as potent GDIs. The structures of the LGN GL3 and GL4 in complex with Gα$_i$ suggest that both the double-arginine finger and the short variable tail of the GL peptides are important for their GDI activities. The di-arginine finger makes extensive salt bridges with the phosphates of GDP, and the GDP in return makes contacts with both the Ras-like and all-helical domains of Gα$_i$. The variable C-terminal tail of the GL peptides further interacts with the all-helical domain of Gα$_i$. Thus, in addition to stabilizing GDP bound to Gα$_i$, the binding of GL peptide further promotes the closed conformation of Gα$_i$ (*i.e.*, by restricting the opening of the all-helical domain and subsequent dissociation of GDP from Gα$_i$; Fig. 7).

The characteristic multiple GLs in LGN and its *Drosophila* homolog Pins have been implicated to play a role in regulating their intramolecular interactions between TPR repeats and GLs

in response to the binding of Gα$_i$·GDP and NuMA/Mud (34, 43). In addition to this, the multiple GLs in LGN (Pins) also function as a scaffold in regulating the localization of related protein complexes and organizing signaling pathways mediating spindle orientations. The detailed characterizations of interactions between LGN-GLs and Gα$_i$·GDP in this work demonstrate that in its open state the four LGN GLs have equal capacity to bind to Gα$_i$·GDP (Fig. 6*E*). In another word, the stoichiometry of LGN/Gα$_i$·GDP complex *in vivo* likely depends on the concentration of Gα$_i$·GDP, which in turn regulates the cortical localization of LGN-bound proteins, such as NuMA. Recently, it was found that the extrinsic GPCR Tre1 signaling determines the orientation of cortical polarity in the asymmetric cell division of *Drosophila* neuroblast (44). Tre1 was shown to activate Gα$_o$, and the GTP form Gα$_o$ can specifically associate with the first GL of Pins (44). Thus, the presence of multiple GLs allows Pins to function as a scaffold to simultaneously engage Gα$_o$- and Gα$_i$-mediated signaling events during asymmetric cell division.

REFERENCES

1. Malbon, C. C. (2005) G proteins in development. *Nat. Rev. Mol. Cell Biol.* **6,** 689–701
2. Sprang, S. R. (1997) G protein mechanisms. Insights from structural analysis. *Annu. Rev. Biochem.* **66,** 639–678
3. Gilman, A. G. (1987) G proteins. Transducers of receptor-generated signals. *Annu. Rev. Biochem.* **56,** 615–649
4. Sunahara, R. K., Dessauer, C. W., and Gilman, A. G. (1996) Complexity and diversity of mammalian adenylyl cyclases. *Annu. Rev. Pharmacol. Toxicol.* **36,** 461–480
5. Singer, W. D., Brown, H. A., and Sternweis, P. C. (1997) Regulation of eukaryotic phosphatidylinositol-specific phospholipase C and phospholipase D. *Annu. Rev. Biochem.* **66,** 475–509
6. Kozasa, T., Jiang, X., Hart, M. J., Sternweis, P. M., Singer, W. D., Gilman, A. G., Bollag, G., and Sternweis, P. C. (1998) p115 RhoGEF, a GTPase activating protein for Gα12 and Gα13. *Science* **280,** 2109–2111
7. Willard, F. S., Kimple, R. J., and Siderovski, D. P. (2004) Return of the GDI. The GoLoco motif in cell division. *Annu. Rev. Biochem.* **73,** 925–951
8. Siderovski, D. P., Diversé-Pierluissi, M., and De Vries, L. (1999) The GoLoco motif. A Gα$_{i/o}$ binding motif and potential guanine-nucleotide exchange factor. *Trends Biochem. Sci.* **24,** 340–341
9. Bernard, M. L., Peterson, Y. K., Chung, P., Jourdan, J., and Lanier, S. M. (2001) Selective interaction of AGS3 with G-proteins and the influence of AGS3 on the activation state of G-proteins. *J. Biol. Chem.* **276,** 1585–1593
10. Kimple, R. J., De Vries, L., Tronchère, H., Behe, C. I., Morris, R. A., Gist Farquhar, M., and Siderovski, D. P. (2001) RGS12 and RGS14 GoLoco motifs are Gα$_i$ interaction sites with guanine nucleotide dissociation inhibitor activity. *J. Biol. Chem.* **276,** 29275–29281
11. Natochin, M., Gasimov, K. G., and Artemyev, N. O. (2001) Inhibition of GDP/GTP exchange on Gα subunits by proteins containing G-protein regulatory motifs. *Biochemistry* **40,** 5322–5328
12. Granderath, S., Stollewerk, A., Greig, S., Goodman, C. S., O'Kane, C. J., and Klämbt, C. (1999) loco encodes an RGS protein required for *Drosophila* glial differentiation. *Development* **126,** 1781–1791
13. Ponting, C. P. (1999) Raf-like Ras/Rap-binding domains in RGS12- and still-life-like signalling proteins. *J. Mol. Med.* **77,** 695–698
14. Kimple, R. J., Kimple, M. E., Betts, L., Sondek, J., and Siderovski, D. P. (2002) Structural determinants for GoLoco-induced inhibition of nucleotide release by Gα subunits. *Nature* **416,** 878–881
15. Bosch, D. E., Kimple, A. J., Sammond, D. W., Muller, R. E., Miley, M. J.,

Machius, M., Kuhlman, B., Willard, F. S., and Siderovski, D. P. (2011) Structural determinants of affinity enhancement between GoLoco motifs and G-protein α subunit mutants. *J. Biol. Chem.* **286,** 3351–3358

16. Sammond, D. W., Eletr, Z. M., Purbeck, C., Kimple, R. J., Siderovski, D. P., and Kuhlman, B. (2007) Structure-based protocol for identifying mutations that enhance protein-protein binding affinities. *J. Mol. Biol.* **371,** 1392–1404

17. Sammond, D. W., Bosch, D. E., Butterfoss, G. L., Purbeck, C., Machius, M., Siderovski, D. P., and Kuhlman, B. (2011) Computational design of the sequence and structure of a protein-binding peptide. *J. Am. Chem. Soc.* **133,** 4190–4192

18. Bosch, D. E., Willard, F. S., Ramanujam, R., Kimple, A. J., Willard, M. D., Naqvi, N. I., and Siderovski, D. P. (2012) A P-loop mutation in Gα subunits prevents transition to the active state. Implications for G-protein signaling in fungal pathogenesis. *PLoS Pathog.* **8,** e1002553

19. Du, Q., Stukenberg, P. T., and Macara, I. G. (2001) A mammalian partner of inscuteable binds NuMA and regulates mitotic spindle organization. *Nat. Cell Biol.* **3,** 1069–1075

20. Zhu, J., Wen, W., Zheng, Z., Shang, Y., Wei, Z., Xiao, Z., Pan, Z., Du, Q., Wang, W., and Zhang, M. (2011) LGN/mInsc and LGN/NuMA complex structures suggest distinct functions in asymmetric cell division for the Par3/mInsc/LGN and Gαi/LGN/NuMA pathways. *Mol. Cell* **43,** 418–431

21. Du, Q., Taylor, L., Compton, D. A., and Macara, I. G. (2002) LGN blocks the ability of NuMA to bind and stabilize microtubules. A mechanism for mitotic spindle assembly regulation. *Curr. Biol.* **12,** 1928–1933

22. Du, Q., and Macara, I. G. (2004) Mammalian Pins is a conformational switch that links NuMA to heterotrimeric G proteins. *Cell* **119,** 503–516

23. Siller, K. H., Cabernard, C., and Doe, C. Q. (2006) The NuMA-related Mud protein binds Pins and regulates spindle orientation in *Drosophila* neuroblasts. *Nat. Cell Biol.* **8,** 594–600

24. Izumi, Y., Ohta, N., Hisata, K., Raabe, T., and Matsuzaki, F. (2006) *Drosophila* Pins-binding protein Mud regulates spindle-polarity coupling and centrosome organization. *Nat. Cell Biol.* **8,** 586–593

25. Bowman, S. K., Neumüller, R. A., Novatchkova, M., Du, Q., and Knoblich, J. A. (2006) The *Drosophila* NuMA homolog Mud regulates spindle orientation in asymmetric cell division. *Dev. Cell* **10,** 731–742

26. Colombo, K., Grill, S. W., Kimple, R. J., Willard, F. S., Siderovski, D. P., and Gönczy, P. (2003) Translation of polarity cues into asymmetric spindle positioning in *Caenorhabditis elegans* embryos. *Science* **300,** 1957–1961

27. Gotta, M., Dong, Y., Peterson, Y. K., Lanier, S. M., and Ahringer, J. (2003) Asymmetrically distributed *C. elegans* homologs of AGS3/PINS control spindle position in the early embryo. *Curr. Biol.* **13,** 1029–1037

28. Srinivasan, D. G., Fisk, R. M., Xu, H., and van den Heuvel, S. (2003) A complex of LIN-5 and GPR proteins regulates G protein signaling and spindle function in *C. elegans. Genes Dev.* **17,** 1225–1239

29. Bellaïche, Y., Radovic, A., Woods, D. F., Hough, C. D., Parmentier, M. L., O'Kane, C. J., Bryant, P. J., and Schweisguth, F. (2001) The partner of Inscuteable/Discs-large complex is required to establish planar polarity during asymmetric cell division in *Drosophila. Cell* **106,** 355–366

30. Sans, N., Wang, P. Y., Du, Q., Petralia, R. S., Wang, Y. X., Nakka, S., Blumer, J. B., Macara, I. G., and Wenthold, R. J. (2005) mPins modulates PSD-95 and SAP102 trafficking and influences NMDA receptor surface expression. *Nat. Cell Biol.* **7,** 1179–1190

31. Zhu, J., Shang, Y., Xia, C., Wang, W., Wen, W., and Zhang, M. (2011) Guanylate kinase domains of the MAGUK family scaffold proteins as specific phospho-protein-binding modules. *EMBO J.* **30,** 4986–4997

32. Yu, F., Kuo, C. T., and Jan, Y. N. (2006) *Drosophila* neuroblast asymmetric cell division. Recent advances and implications for stem cell biology. *Neuron* **51,** 13–20

33. Kaushik, R., Yu, F., Chia, W., Yang, X., and Bahri, S. (2003) Subcellular localization of LGN during mitosis. Evidence for its cortical localization in mitotic cell culture systems and its requirement for normal cell cycle progression. *Mol. Biol. Cell* **14,** 3144–3155

34. Nipper, R. W., Siller, K. H., Smith, N. R., Doe, C. Q., and Prehoda, K. E. (2007) Gα_i generates multiple Pins activation states to link cortical polarity and spindle orientation in *Drosophila* neuroblasts. *Proc. Natl. Acad. Sci. U.S.A.* **104,** 14306–14311

35. Otwinowski, Z., and Minor, W. (1997) Methods in Enzymology, Vol. 276, pp. 307–326, Elsevier, New York

36. Vagin, A., and Teplyakov, A. (1997) MOLREP: an automated program for molecular replacement. *J. Appl. Crystallogr.* **30,** 1022–1025

37. Murshudov, G. N., Vagin, A. A., and Dodson, E. J. (1997) Refinement of macromolecular structures by the maximum-likelihood method. *Acta Crystallogr. D* **53,** 240–255

38. Adams, P. D., Afonine, P. V., Bunkóczi, G., Chen, V. B., Davis, I. W., Echols, N., Headd, J. J., Hung, L. W., Kapral, G. J., Grosse-Kunstleve, R. W., McCoy, A. J., Moriarty, N. W., Oeffner, R., Read, R. J., Richardson, D. C., Richardson, J. S., Terwilliger, T. C., and Zwart, P. H. (2010) PHENIX. A comprehensive Python-based system for macromolecular structure solution. *Acta Crystallogr. D Biol. Crystallogr.* **66,** 213–221

39. Emsley, P., and Cowtan, K. (2004) Coot. Model-building tools for molecular graphics. *Acta Crystallogr. D* **60,** 2126–2132

40. McCudden, C. R., Willard, F. S., Kimple, R. J., Johnston, C. A., Hains, M. D., Jones, M. B., and Siderovski, D. P. (2005) Gα selectivity and inhibitor function of the multiple GoLoco motif protein GPSM2/LGN. *Biochim. Biophys. Acta* **1745,** 254–264

41. Adhikari, A., and Sprang, S. R. (2003) Thermodynamic characterization of the binding of activator of G protein signaling 3 (AGS3) and peptides derived from AGS3 with Gα_{i1}. *J. Biol. Chem.* **278,** 51825–51832

42. Kopein, D., and Katanaev, V. L. (2009) *Drosophila* GoLoco-protein Pins is a target of Gα_o-mediated G protein-coupled receptor signaling. *Mol. Biol. Cell* **20,** 3865–3877

43. Smith, N. R., and Prehoda, K. E. (2011) Robust spindle alignment in *Drosophila* neuroblasts by ultrasensitive activation of pins. *Mol. Cell* **43,** 540–549

44. Yoshiura, S., Ohta, N., and Matsuzaki, F. (2012) Tre1 GPCR signaling orients stem cell divisions in the *Drosophila* central nervous system. *Dev. Cell* **22,** 79–91

45. Chen, V. B., Arendall, W. B., 3rd, Headd, J. J., Keedy, D. A., Immormino, R. M., Kapral, G. J., Murray, L. W., Richardson, J. S., and Richardson, D. C. (2010) MolProbity. All-atom structure validation for macromolecular crystallography. *Acta Crystallogr. D Biol. Crystallogr.* **66,** 12–21